PHYSICAL REVIEW A VOLUME 36, NUMBER 10 NOVEMBER 15, 1987

Soft-sphere model for the glass transition in binary alloys: Pair structure and self-diffusion

B. Bernu and J. P. Hansen
Laboratoire de Physique Théorique des Liquides, Université Pierre et Marie Curie, 75252 Paris Cédex 05, France

Y. Hiwatari
Department of Physics, Faculty of Science, Kanazawa University, Kanazawa, Ishikawa 920, Japan

G. Pastore*
Laboratoire de Physique Théorique des Liquides, Université Pierre et Marie Curie, 75252 Paris Cédex 05, France
(Received 27 January 1987; revised manuscript received 21 May 1987)

Molecular-dynamics simulations have been carried out on a "soft-sphere" model for binary alloys quenched into supercooled and amorphous states. The main emphasis of the work is on the static and dynamic characterization of the glass transition. A comparison between molecular-dynamics data and the results of a self-consistent integral equation shows that the equation of state bifurcates into "glass" and "fluid" branches below a glass transition temperature T_g. The static pair structures differ significantly along the two branches. The structurally relaxed "fluid" branch leads to a phase separation at very low temperatures. Close to the glass transition, the atomic mean-square displacements of the two species go over more and more slowly to the asymptotic diffusive regime, due to the emergence of an intermediate time scale linked to the slowing down of structural relaxation. The diffusion constants of the two species follow closely a scaling law, as predicted by mode-coupling theory, except in the immediate vicinity of the glass transition where activated processes lead to residual diffusion.

I. INTRODUCTION

The glass transition from a supercooled liquid to a frozen amorphous state is readily observed in the laboratory for complex multicomponent systems, polymers, or network-forming substances, but the practically achievable cooling rates are not sufficient to bypass crystallization and obtain a glass phase of simple atomic systems, like rare gases or pure liquid metals. However, simple model systems of spherical particles can be quenched into amorphous solid states in molecular-dynamics (MD) or Monte Carlo "computer experiments,"[1] where cooling rates are typically 10^{11} K/sec or higher.[2,3] Such a "computer glass" shares many characteristic features with glasses obtained in the laboratory, but lends itself more readily to theoretical analysis. Recent theoretical developments, based on the mode-coupling techniques of the theory of liquids,[4] point to the essentially dynamical origin of the glass transition.[5–9] These theories focus on the density-density correlation function, the decay of which is found to exhibit two slow relaxation time scales in the supercooled liquid phase. The glass transition is signaled by the divergence of the structural relaxation time and a resulting non-ergodic behavior characteristic of "structural arrest." These predictions appear to be borne out by recent MD simulations of the density-density correlation function of a supercooled Lennard-Jones system.[10] However, a more quantitative confrontation with theory would require very long simulation runs (typically $> 10^4$ time steps in a MD "experiment") in order to probe the slow decay mechanisms; this is difficult to achieve with simple one-component systems, since the supercooled fluid always exhibits a tendency towards nucleation over sufficiently long time intervals.[11]

Nucleation is much more easily bypassed in quenched samples of binary mixtures of spherical particles with different diameters.[12] This situation is reminiscent of the ease with which certain metallic alloys can be quenched into stable amorphous states by a variety of fast cooling techniques. The model which we consider in this paper is a binary mixture of "soft spheres" containing two species of spherical particles of different diameters which interact through purely repulsive inverse power potentials. Our preliminary simulations,[12] as well as the more extensive calculations presented in the present paper, showed no sign of a tendency towards crystallization of the quenched computer samples, even for the longest runs, thus allowing a detailed study of slow relaxations near the glass transition.

The advantage of considering a simple inverse power potential model is twofold. First, the corresponding mixtures have simple scaling properties which imply a reduction of the number of independent thermodynamical variables from 3 to 2; as a consequence, compression and cooling of the samples constitute equivalent routes towards glass formation. On the other hand, the one-component version of the soft-sphere model has been extensively studied by MD and Monte Carlo simulations, both in the stable fluid and crystal phases,[13–15] and in the supercooled and amorphous states.[11,16,17] The generalization of the model to binary mixtures, which is the subject of this paper, can be regarded as the simplest

model, retaining the essential features of glass-forming alloys, such as Ag-Cu or Cu-Mg films.

Although the main motivation of our simulation work remains the dynamic characterization of the glass transition, we also present and analyze static properties of the supercooled and amorphous mixtures, including the equation of state, the pair structure, and the tendency towards segregation of the two species. The static properties for several concentrations were calculated by constant-energy and constant-temperature MD simulations, and from numerical solutions of a thermodynamically self-consistent integral equation for the pair structure.[18] In the second part of the paper we examine in detail how the slow structural relaxation affects the self-diffusion of the two species in the vicinity of the glass transition. The relaxation of the density-density correlation function will be the subject of a subsequent paper.

II. THE MODEL

We consider binary mixtures of N_1 atoms of mass m_1 and diameter σ_1 and N_2 atoms of mass m_2 and diameter σ_2 in a volume V. They interact through the purely repulsive soft-sphere potentials:

$$v_{\alpha\beta}(r)=\epsilon\left[\frac{\sigma_{\alpha\beta}}{r}\right]^{12}, \tag{1a}$$

where $1\leq\alpha,\beta\leq 2$ are species indexes, and the diameters are assumed to be additive, i.e.,

$$\sigma_{\alpha\beta}=\tfrac{1}{2}(\sigma_\alpha+\sigma_\beta)\ . \tag{1b}$$

According to the scaling property of inverse power potentials, all reduced equilibrium properties of such mixtures, in excess of their ideal gas counterparts, depend only on two independent variables. If $\rho^*=N\sigma_l^3/V$ denotes the reduced number density (with $N=N_1+N_2$), and $T^*=k_BT/\epsilon$ the reduced temperature, the two independent variables are conveniently chosen to be the dimensionless coupling constant[3,4]

$$\Gamma=\rho^*(T^*)^{-1/4}\ , \tag{2}$$

and the number concentration of species l, $x_1=N_1/N$. It is tempting to relate the thermodynamic properties of such a mixture to those of an effective one-component system in the framework of an approximate "one-fluid" description. According to conformal solution theory,[4] the diameter of the atoms in the effective one-component system is given by

$$\sigma_x^3=\sum_\alpha\sum_\beta x_\alpha x_\beta\sigma_{\alpha\beta}^3\ , \tag{3}$$

and the corresponding effective coupling constant is

$$\Gamma_{\rm eff}=\Gamma\left[\frac{\sigma_x}{\sigma_1}\right]^3\ . \tag{4}$$

$\Gamma_{\rm eff}$ depends on concentration and interpolates between the coupling constants relevant for the pure phases at a given temperature and number density, $\Gamma_1=\Gamma$ for x_1-1 and $\Gamma_2=\Gamma(\sigma_2/\sigma_1)^3$ for $x_1=0$ ($x_2=1$).

The freezing point of these pure phases is at $\Gamma_\alpha\simeq 1.15$ ($\alpha=1,2$) (Refs. 13 and 14), while the glass transition is situated around $\Gamma_\alpha=1.5$.[12,16,17] It is worth pointing out that, for a fixed temperature, the density range of the supercooled liquid phase is considerably larger for soft spheres than for hard spheres.

The microscopic time scale is chosen to be

$$\tau=\left[\frac{m_1\sigma_1^2}{12\epsilon}\right]^{1/2}\ . \tag{5}$$

Most of the MD simulations were carried out at constant total energy, using a finite difference algorithm, derived from that recently developed by one of us,[19] to integrate the coupled equations of motion of the N atoms. If Δt denotes the time step in the integration, the particle positions are calculated with an error $O(\Delta t^6)$ by a symmetrized version of the algorithm in Ref. 19; the resulting total energy turns out to be remarkably constant, with a reduced time step $\Delta t^*=\Delta t/\tau\simeq 0.04$, the drift not exceeding 0.02% over 10^4 time steps in the worst cases. Since the temperature fluctuates in constant-energy simulations, which may lead to "blurring" of some dynamical signatures of the glass transition, we have, for comparative purposes, carried out a few constant-temperature (i.e., constant kinetic energy) simulations, using the constraint method of Hoover *et al.* and Nosé.[20,21] Most simulations were done for samples of $N=500$ atoms (with the usual periodic boundary conditions), but two runs were also made for samples of 4000 atoms. We examined only one size ratio, $\sigma_2/\sigma_1=1.4$; most calculations were for a mass ratio $m_2/m_1=2$, with a few runs for a ratio $m_2/m_1=4$. The simulations cover a wide range of states in the stable and supercooled fluid phase and in the glass phase, extending roughly from $\Gamma_{\rm eff}\simeq 1$ to $\Gamma_{\rm eff}\simeq 2.5$, for $x_1=1$, 0.9, 0.75, 0.5, and 0.25, with special emphasis on the equimolar concentration; the characteristics of the various runs are summarized in Table I.

In practice, all simulations were carried out for a reduced number density, such that $\rho^*[x_1+x_2(\sigma_2/\sigma_1)^3]=1$. An equilibrium fluid configuration (at a temperature above the freezing temperature) was obtained by melting an initial crystal configuration. Supercooled and glassy states were obtained from the equilibrium fluid configuration by a succession of quenches during which the velocities of all atoms were scaled down according to $\mathbf{v}_i=\alpha\mathbf{v}_i$, with $0<\alpha\ll 1$. The resulting (instantaneous) change in total energy is simply

$$\Delta E=\tfrac{1}{2}\sum_i m_i v_i^2(1-\alpha^2)=\tfrac{3}{2}Nk_B(T_1-T_1')\ . \tag{6}$$

The isolated system is then left to evolve in time to a new temperature T_2, with a redistribution of ΔE among the kinetic and potential components of the total energy. A very dense system is not far from harmonic, so that equipartition holds approximately; consequently,

$$\Delta E\simeq 2\times\tfrac{3}{2}Nk_B(T_1-T_2)\ . \tag{7}$$

Comparison of Eqs. (6) and (7) leads to the estimate of the final temperature:

$$T_2\simeq(T_1+T_1')/2\simeq T_1/2\ \text{ as }\alpha\to 0\ . \tag{8}$$

TABLE I. Summary of molecular-dynamics runs. The column MD specifies constant-energy (E) or constant-temperature (T) simulations; $\Delta t^* = \Delta t/\tau$ is the time step and N_t is the total number of time steps, including equilibration.

MD	N_1	N_2	m_2/m_1	x_1	T^*	Γ_{eff}	Δt^*	$N_t/10^3$	$\beta P/\rho$
E	250	250	2	0.5	1.065	0.947	0.018	2+5	12.60
E	500	0		1.0	0.611	1.131	0.030	4+4	18.71
E	250	250	2	0.5	0.501	1.143	0.035	4+4	20.22
E	250	250	2	0.5	0.482	1.154	0.022	2+10	20.80
E	125	375	2	0.25	0.509	1.156	0.035	4+4	20.48
E	375	125	2	0.75	0.423	1.192	0.035	4+4	22.65
E	250	250	2	0.5	0.384	1.221	0.035	4+4	24.19
E	250	250	4	0.5	0.359	1.242	0.035	4+4	25.34
E	250	250	2	0.5	0.319	1.280	0.035	4+4	27.66
E	250	250	2	0.5	0.256	1.352	0.035	2+10	32.41
E	450	50	2	0.9	0.255	1.376	0.040	4+4	32.88
E	250	250	2	0.5	0.211	1.418	0.035	4+4	37.69
E	250	250	2	0.5	0.208	1.425	0.035	2+20	37.87
T	250	250	2	0.5	0.207	1.425	0.035	2+10	38.09
E	250	250	4	0.5	0.193	1.451	0.050	4+4	40.43
E	2000	2000	2	0.5	0.190	1.457	0.040	2+2	40.95
E	250	250	2	0.5	0.172	1.494	0.050	4+4	44.41
E	250	250	2	0.5	0.165	1.508	0.050	4+4	45.66
E	250	250	4	0.5	0.164	1.511	0.050	4+4	46.07
E	250	250	2	0.5	0.159	1.523	0.035	2+20	47.03
T	250	250	2	0.5	0.159	1.523	0.035	2+10	47.35
E	250	250	2	0.5	0.151	1.543	0.035	4+4	49.41
E	125	375	2	0.25	0.150	1.570	0.055	4+4	51.33
T	250	250	2	0.5	0.136	1.584	0.035	2+10	53.98
E	250	250	2	0.5	0.135	1.586	0.035	2+20	53.91
E	375	125	2	0.75	0.128	1.608	0.040	4+4	56.58
E	216	216	2	0.5	0.127	1.612	0.040	4+4	53.50
	(CsCl crystal)								
E	450	50	2	0.9	0.129	1.631	0.040	4+4	57.71
E	500	0		1.0	0.133	1.656	0.050	4+4	54.00
T	250	250	2	0.5	0.110	1.670	0.035	10+20	65.01
E	2000	2000	2	0.5	0.101	1.705	0.050	2+2	70.40
E	250	250	2	0.5	0.090	1.755	0.050	4+4	78.25
E	250	250	2	0.5	0.060	1.943	0.050	4+4	114.4
E	375	125	2	0.75	0.040	2.153	0.070	4+4	168.1
E	250	250	2	0.5	0.033	2.263	0.100	4+4	205.3
E	375	125	2	0.75	0.024	2.445	0.100	4+4	274.4

The process can be repeated several times to reach quenched states of arbitrarily low temperature. Two successive quenches are typically separated by 10^2 time steps. Intermediate temperatures can be achieved by adjusting the scaling factor α accordingly.

A common feature of the constant-energy simulations is the slow upward drift of the temperature (i.e., total kinetic energy) observed for most glassy states (i.e., for $\Gamma_{\text{eff}} \gtrsim 1.5$); the drift represents typically less than 1% of the initial temperature (after equilibration) in a 4000 time-step run, and appears to slow down with time in most cases. However, there is almost no drift of the pressure along the run. There is a corresponding downward drift in total energy in the isothermal simulations.

III. THE EQUATION OF STATE

The excess internal energy U of the soft-sphere mixture is calculated from the statistical average of the total potential energy V_N, while the pressure P, as calculated from the virial theorem, is directly proportional to U for inverse-power potentials; in the present case,

$$\frac{\beta P}{\rho} - 1 = 4\frac{\beta U}{N} = \frac{4}{Nk_B T}\langle V_N \rangle \ . \tag{9}$$

The MD estimates of the equation of state $\beta P/\rho$ are listing in Table I and plotted versus Γ_{eff}^4 in Fig. 1. If the one-fluid description were exact, all points, corresponding to different concentrations, would fall on the same

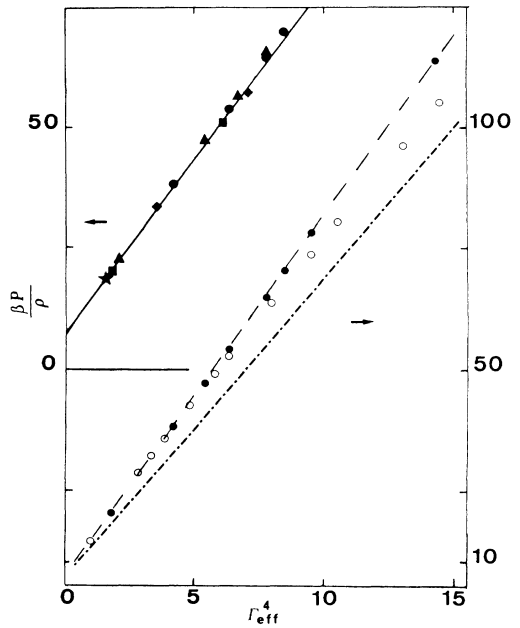

FIG. 1. Equation of state $\beta P/\rho$ of soft-sphere mixtures vs $\Gamma^4_{\rm eff}$. Upper part of figure: MD data (solid symbols) for $x_1=1$ (star), $x_1=0.9$ (diamonds), $x_1=0.75$ (triangles), $x_1=0.5$ (circles), and $x_1=0.25$ (squares); the solid line is the conformal solution equation of state (EOS) (12) (with $b=1.712$). Lower part of figure: equation of state for the concentration $x_1=0.5$; solid circles (linked by dashed line), MD data; open circles, RY results; dashed-dotted line, harmonic EOS (11) (with $b=1.727$) for a CsCl lattice.

curve. This is nearly so, as can be seen from the figure, where all MD results fall practically on a straight line. The linear behavior is easily understood from a simple harmonic model for high-density (or low-temperature) states; according to this model,

$$\frac{U}{N}=a(x_1)\epsilon(\rho^*)^4+\tfrac{3}{2}k_BT+O(T^2)\ , \tag{10}$$

where $a(x_1)$ is a concentration-dependent Madelung constant which determines the zero-temperature "lattice" energy. The corresponding equation of state reads

$$\frac{\beta P}{\rho}-1=6+4a(x_1)\Gamma^4\ . \tag{11}$$

In the one-component case ($x_1=1$), $a=1.450$ for the fcc lattice, while the equation of state of the supercooled liquid and glass phase is very well fitted by Eq. (11) with $a=1.712$.[16] In light of the results shown in Fig. 1, the equation of state of the amorphous mixture is most efficiently written in the form

$$\frac{\beta P}{\rho}=7+4b(x_1)\Gamma^4_{\rm eff}\ , \tag{12}$$

where most of the concentration dependence is contained in $\Gamma_{\rm eff}$, so that $b=a(\sigma_1/\sigma_x)^{12}$ is only weakly dependent on x_1. In the one-fluid approximation, b is independent of x_1 and equal to the value $a=1.712$ found for the one-component case; the deviations from this approximation are found to be small, but significant. A least-squares fit to the equimolar amorphous data ($x_1=0.5$) yields $b=1.88$, while the corresponding Madelung constant for the crystalline CsCl structure (which appears to be the most stable for a ratio $\sigma_2/\sigma_1=1.4$) is $b=1.727$.

The equation of state was also calculated from a straightforward multicomponent generalization of a thermodynamically self-consistent integral equation due to Rogers and Young (RY),[18,22] which will be presented in greater detail in Sec. IV. The RY equation yields equations of state which agree very closely (within better than 1%) with simulation data over the whole fluid range of all inverse-power potentials, and in particular for the present soft-sphere model. Our own calculations show that this excellent agreement extends into the supercooled fluid range for all concentrations up to $\Gamma_{\rm eff}\simeq 1.5$. Beyond that coupling a clear bifuraction is observed, as shown in Fig. 1 for an equimolar mixture: The RY results drop progressively below the MD data as Γ increases. This trend could be attributed to a gradual breakdown of the RY closure under very strong coupling conditions, but this does not seem to be very likely, since different implementations of the thermodynamic self-consistency requirement (to be discussed in Sec. IV) lead to nearly identical results, as shown in Table II. We believe that the different pressures correspond to two physically different branches of the equation of state. The upper branch, along which the MD data lie, may be associated with typical glassy states, i.e., quenched metastable structures which were unable to relax within the duration of the MD runs, since structural relaxation times increase by many orders of magnitude beyond the glass transition ("structural arrest"). This branch is of course not unique and may depend, among other factors, on the cooling rate during the preparation of the initial configuration of the sample. Also the point beyond which bifurcation occurs will depend on the initial preparation. It is, however, worth stressing that all the MD-generated "glassy" states appear to fall on the same curve, independently of the initial preparation and nearly independently of concentration, at least within the limited range of initial configurations and cooling rates which we have explored.

The lower branch drawn through the RY results, on the other hand, corresponds to metastable disordered states of lowest free energy, since the integral equation describes translationally invariant "equilibrium" situations which would be reached after a sufficiently long structural relaxation process. True thermodynamic equilibrium can only be reached by translational symmetry-breaking nucleation into the crystal phase, which is characterized by significantly lower pressures, as shown in Fig. 1.

The bifurcation in the equation of state, and the ensuing difference in slopes beyond the glass transition is reminiscent of the distinct "kinks" in the variation of a number of thermodynamic properties with temperature at constant pressure observed in many simulations of one-component systems. The soft-sphere model under

TABLE II. Thermodynamic results from HNC and three versions of the self-consistent RY integral equation, for two states of an equimolar soft-sphere mixture; when two results are given, the first is obtained via the virial route, while the second stems from the compressibility (or fluctuation) route; χ_T is the isothermal compressibility while v_1 and v_2 are the partial molar volumes.

	HNC	RY1	RY2	RY3	MD
		$x_1=0.5$; $T^*=0.207$; $\Gamma_{\text{eff}}=1.425$			
$\rho k_B T\chi_T$	5.9	6.54	6.54	6.54	6.15
$\times 10^3$	11.4	6.54	6.54	6.54	6.3±0.3
$\beta P/\rho$	42.64	37.81	37.75	37.80	38.0
$\beta v_1/\chi_T$	109.3	97.43	97.70	97.72	
	56.43	98.57	97.27	97.34	
$\beta v_2/\chi_T$	231.4	208.7	207.8	208.3	
	119.5	207.2	211.0	208.6	
$S_{CC}(0)/x_1x_2$	1.64	1.41	1.49	1.33	
		$x_1=0.5$; $T^*=0.107$; $\Gamma_{\text{eff}}=1.68$			
$\rho k_B T\chi_T$	3.37	3.65	3.65	3.65	3.26
$\times 10^3$	6.88	3.65	3.65	3.65	
$\beta P/\rho$	70.90	63.78	63.74	63.76	66.84
$\beta v_1/\chi_T$	188.3	172.6	177.5	173.1	
	92.16	175.4	171.1	172.8	
$\beta v_2/\chi_T$	405.2	375.3	374.4	375.0	
	198.7	372.5	376.7	374.9	
$S_{CC}(0)/x_1x_2$	4.02	2.10	2.39	1.85	

investigation leads to unphysically high pressures, due to the purely repulsive nature of interatomic forces. In order to investigate thermodynamic properties at zero pressure, we have taken into account the effect of attractive interactions within the standard van der Waals mean-field approximation.[23–25] If combined with the equation of state (12), this leads to simple analytic expressions for the thermodynamic properties at constant pressure. The corresponding volume per article, enthalpy, compressibility, and thermal expansion coefficient all exhibit a distinct change in slope at a temperature $T_g^* \simeq 0.3$ which is often identified with the glass transition temperature, and corresponds to a value $\Gamma_{\text{eff}} \simeq 1.5$ of the effective coupling constant, in agreement with the approximate location of the bifurcation point in the equation of state.

IV. PAIR STRUCTURE AND SEGREGATION

The microscopic pair structure of binary mixtures is characterized by three partial pair distribution functions (PDF) $g_{\alpha\beta}(r)$, or equivalently, by their Fourier transforms, the partial structure factors $S_{\alpha\beta}(k)$:

$$S_{\alpha\beta}(k)=\frac{1}{N}\langle \rho_{\mathbf{k}\alpha}\rho^*_{\mathbf{k}\beta}\rangle$$

$$=x_\alpha\delta_{\alpha\beta}+\rho x_\alpha x_\beta \int h_{\alpha\beta}(r)e^{i\mathbf{k}\cdot\mathbf{r}}\,d\mathbf{r}\ , \tag{13}$$

where the $h_{\alpha\beta}(r)=g_{\alpha\beta}(r)-1$ are the correlation functions and

$$\rho_{\mathbf{k}\alpha}=\sum_{i=1}^{N_\alpha} e^{i\mathbf{k}\cdot\mathbf{r}_{i\alpha}},\quad \alpha=1,2 \tag{14}$$

is a Fourier component of the microscopic density of species α. Two linear combinations of $\rho_{\mathbf{k}1}$ and $\rho_{\mathbf{k}2}$ are of particular physical interest, namely, the Fourier components of the total number and concentration densities:

$$\rho_{\mathbf{k}N}=\rho_{\mathbf{k}1}+\rho_{\mathbf{k}2}\ , \tag{15a}$$

$$\rho_{\mathbf{k}C}=x_2\rho_{\mathbf{k}1}-x_1\rho_{\mathbf{k}2}\ . \tag{15b}$$

From these, the three Bhatia-Thornton[26] structure factors $S_{NN}(k)$, $S_{NC}(k)$, and $S_{CC}(k)$ are defined by relations similar to Eq. (15); they are obviously linear combinations of the three partial structure factors; their long-wavelength limits are related to second derivatives of the Gibbs free energy G; in particular

$$\lim_{k\to 0} S_{CC}(k)=\frac{Nk_BT}{(\partial^2 G/\partial x_1^2)_{T,P,N}}\ . \tag{16}$$

The MD simulations yield accurate estimates of the PDF $g_{\alpha\beta}(r)$ for distances r less than half the length L of the simulation cell. Truncation of the Fourier integral in Eq. (13) leads to spurious results for the corresponding $S_{\alpha\beta}(k)$ for $k \lesssim 2\pi/L$, thus preventing a direct evaluation of the $k\to 0$ limit in Eq. (16).

The $g_{\alpha\beta}(r)$ and $S_{\alpha\beta}(k)$ can also be obtained from numerical solutions of the familiar integral equations of the

theory of liquids.[4] The classic Percus-Yevick and hypernetted-chain (HNC) equations suffer from internal thermodynamic inconsistency, which can be overcome by a number of improvement schemes. One of the most successful is the interpolation scheme of Rogers and Young,[18] which has the merit of being easily generalized to the case of mixtures.[22] The RY integral equation supplements the three Ornstein-Zernike relations between the $h_{\alpha\beta}(r)$ and the direct correlation functions $c_{\alpha\beta}(r)$ by the closure relations

$$g_{\alpha\beta}(r)=\exp[-\beta v_{\alpha\beta}(r)]\left[1+\frac{\exp\{f_{\alpha\beta}(r)[h_{\alpha\beta}(r)-c_{\alpha\beta}(r)]\}-1}{f_{\alpha\beta}(r)}\right], \tag{17}$$

where the $f_{\alpha\beta}(r)$ are "switching functions" conveniently taken in the form[18]

$$f_{\alpha\beta}(r)=1-\exp(-\xi_{\alpha\beta}r)\ . \tag{18}$$

The parameters $\xi_{\alpha\beta}$ are adjusted to ensure thermodynamic consistency of the integral equation. In the one-component case, the single parameter ξ is adjusted to achieve self-consistency between the virial and compressibility (fluctuation) routes to the equation of state. For a two-component system, there are three parameters $\xi_{\alpha\beta}$, but only two consistency conditions, namely,

$$\left[\frac{\partial\beta P}{\partial\rho_\alpha}\right]_{T,\rho_{\alpha'}}=1-\sum_\beta \rho_\beta \hat{c}_{\alpha\beta}(k=0),\quad \alpha=1,2 \tag{19}$$

where $\hat{c}_{\alpha\beta}(k)$ denotes the Fourier transform of $c_{\alpha\beta}(r)$; in a self-consistent theory the left-hand side of Eq. (19), with the pressure calculated from the virial equation, must coincide with the fluctuation result on the right-hand side. In the simplest version of RY theory (RY1) applied to binary mixtures,[22] a single parameter ξ is used (i.e., $\xi_{11}=\xi_{12}=\xi_{22}=\xi$), and this is determined from the single condition obtained by summing the two conditions (19), namely,

$$(\rho k_B T\chi_T)^{-1}=\left[\frac{\partial\beta p^{\rm vir}}{\partial\rho}\right]_{T,x_1}=1-\sum_\alpha\sum_\beta x_\alpha x_\beta \rho\hat{c}_{\alpha\beta}\ (k=0)\ . \tag{20}$$

More generally, if the characteristic scales of the $g_{\alpha\beta}(r)$ (e.g., the positions of the main peaks) are denoted by $R_{\alpha\beta}$, the ordering $R_{11}<R_{12}<R_{22}$ leads us to expect that the reciprocal lengths $\xi_{\alpha\beta}$ should be ordered according to $\xi_{22}<\xi_{12}<\xi_{11}$. Only one consistency relation [namely, Eq. (20)] is needed if the following constraint is imposed:

$$\frac{\xi_{11}}{\xi_{12}}=\frac{R_{12}}{R_{11}},\quad \frac{\xi_{22}}{\xi_{12}}=\frac{R_{12}}{R_{22}}\ \text{(RY2)}\ . \tag{21}$$

If the two consistency relations (19) are used, the number of independent parameters $\xi_{\alpha\beta}$ is restricted to two, by imposing the constraint

$$\frac{\xi_{11}}{\xi_{12}}=1+\epsilon,\quad \frac{\xi_{22}}{\xi_{12}}=1-\epsilon\ \text{(RY3)}\ . \tag{22}$$

A typical comparison of thermodynamic properties, calculated via each of these RY routes, and via the HNC approximation (where $\xi_{\alpha\beta}=\infty$), is made in Table II for two equimolar states, one above and one below the glass transition temperature. The three RY schemes yield nearly identical pressures and good internal consistency between the virial and fluctuation routs for those quantities that are not directly tied by the consistency relations. This contrasts sharply with the high degree of inconsistency of the HNC results. As already noted in the Sec. II, the RY pressures are very close to the MD result at the temperature above the glass transition, while they lie 5% below the MD result at the lower temperature.

The quantity which is most sensitive to small variations of the $\xi_{\alpha\beta}$ is the long-wavelength limit of $S_{CC}(k)$. Despite the resulting uncertainties on $S_{CC}(k=0)$, this quantity is found to increase rapidly, and appears to diverge, as the temperature is lowered well below the glass transition temperature T_g^*. According to the result (16) this divergence signals the limit of stability of the mixture against phase separation, since the spinodal line is precisely determined by the condition $\partial^2 G/\partial x_1^2=0$. The situation is illustrated in Fig. 2 for three concentrations;. the demixing tendency is seen to be particularly strong for low concentrations of the larger species. Phase separation is also obtained for less dissymmetric mixtures (e.g., for $\sigma_2/\sigma_1=1.2$), but at considerably lower temperatures. No such demixing is observed in the MD simulations, because the very slow structural relaxation inhibits any tendency towards segregation.

The difference between the "glass" and "fluid" branches is also clearly apparent from the PDF $g_{\alpha\beta}(r)$. Figure 3 shows that above T_g^*, the MD and RY results are very close. Note that the characteristic splitting of

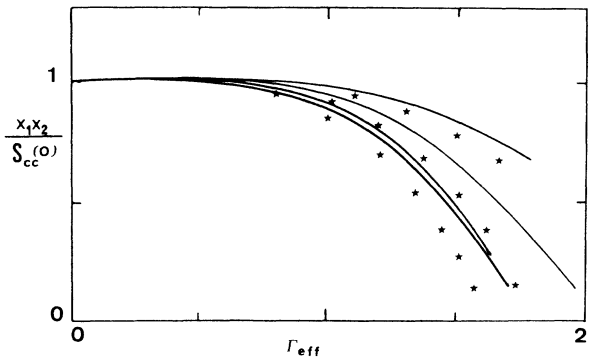

FIG. 2. $x_1x_2/S_{CC}(k=0)$ vs $\Gamma_{\rm eff}$. The solid curves from top to bottom are the RY1 results for $x_1=0.25$, 0.5, 0.9, and 0.75; the stars are the HNC results for $x_1=0.25$, 0.5, and 0.75.

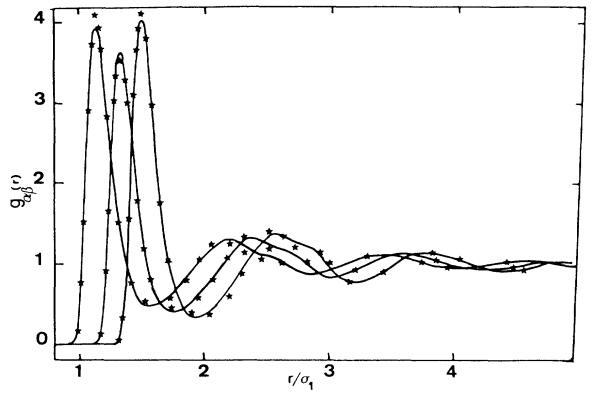

FIG. 3. Partial pair distribution functions $g_{\alpha\beta}(r)$ for $x_1=\frac{1}{2}$, $\Gamma_{\text{eff}}=1.42$. The solid curves are the RY1 results, while stars are MD data.

the second peak of the $g_{\alpha\beta}(r)$ is observed well before the glass transition is reached and cannot, consequently, be considered as a "signature" of that transition. Another noteworthy feature lies in the relative amplitudes of the main peaks of the $g_{\alpha\beta}(r)$: The g_{12} peak is significantly lower than g_{11} and g_{22}, signaling a tendency towards homocoordination; this may be interpreted as a precursor to the phase separation at much lower temperatures. The situation changes considerably well below the glass transition temperature, as illustrated in Fig. 4. The MD and RY results, which may be associated with the "glass" and "fluid" branches, differ now considerably. The RY peaks are much higher and slightly shifted to larger r compared to the MD counterparts; they also show an enhanced tendency towards homocoordination and an almost complete separation between first and second shells, as materialized by nearly vanishing values of the $g_{\alpha\beta}^{\text{RY}}(r)$ between the first and second peaks. The differences between the main peaks of the $g_{\alpha\beta}^{\text{MD}}(r)$ and the corresponding $g_{\alpha\beta}^{\text{RY}}(r)$ show up very clearly in the coordination numbers, calculated according to

$$n_{\alpha\beta}=4\pi\rho_\beta\int_0^{r_{\alpha\beta}} g_{\alpha\beta}(r)r^2\,dr\ , \tag{23}$$

where $r_{\alpha\beta}$ is the position of the first minimum in $g_{\alpha\beta}(r)$.

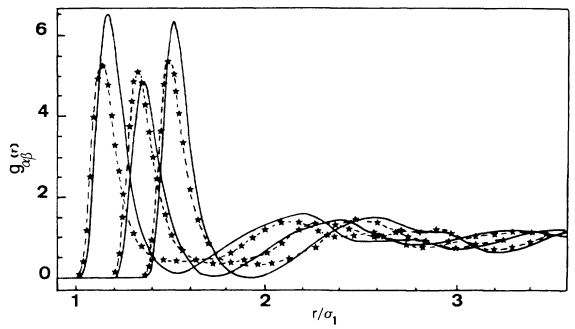

FIG. 4. Same as Fig. 3, but for $\Gamma_{\text{eff}}=1.94$; the dashed curves through the MD data are for visual clarity.

Results for equimolar mixtures are shown in Fig. 5 versus coupling. Whereas the MD data are practically independent of temperature, the RY results for the coordination numbers n_{11} and n_{22} along the "fluid" branch increase significantly with coupling, thus stressing the tendency towards segregation.

Typical examples of Bhatia-Thornton structure factors from MD simulations (on the "glass" branch) and from RY calculations (on the fluid branch) are shown in Figs. 6 and 7. As already stressed earlier, the MD data are not reliable at small k, but the structure factors appear to vary smoothly as $k\to 0$. On the other hand, the RY structure factors increase sharply in that limit, due to the tendency towards segregation in the fluid phase at low temperatures. The MD and RY results for $S_{NN}(k)$ both exhibit a striking "interference" effect in the intermediate wave-number range ($k\sigma_1\simeq 20$): The oscillations in $S_{NN}(k)$ are first damped with increasing k, but after going through a minimum, their amplitude increases again before finally decreasing to zero. This behavior is perfectly reproducible in the MD simulations and is observed for equimolar mixtures over the whole range of temperatures typical of the glass ($\Gamma_{\text{eff}}\gtrsim 1.5$); although less pronounced, this behavior is also observed at higher temperatures, in the supercooled liquid. This "interference" effect was not observed at the other concentrations which we have studied, and may be attributed to an interplay of the relative phases of the oscillations in the partial structure factors $S_{\alpha\beta}(k)$, which depend sensitively on the concentration and size ratio. In particular, the effect is much less pronounced for the smaller size ratio $\sigma_2/\sigma_1=1.2$.

V. SELF-DIFFUSION NEAR THE GLASS TRANSITION

One of the most obvious dynamical characterizations of the glass transition is the sharp decrease of the self-diffusion constant D: Except for activated processes

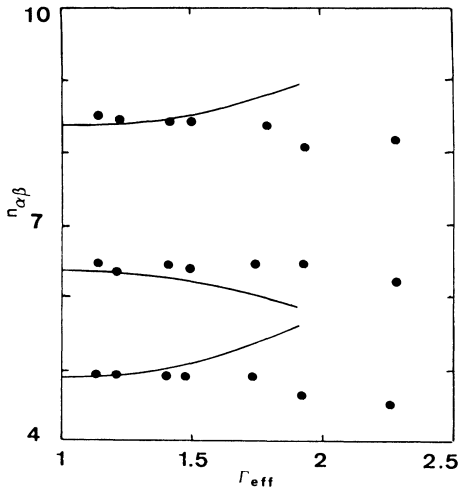

FIG. 5. Coordination numbers n_{11}, n_{12}, and n_{22} (from bottom to top) vs Γ_{eff} for equimolar mixtures. The solid curves are RY1 results, while the dots are the MD data.

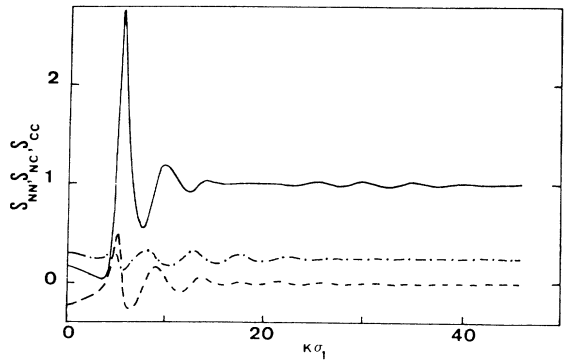

FIG. 6. MD data for the Bhatia-Thornton structure factors $S_{NN}(k)$ (solid curve), $S_{CC}(k)$ (dashed-dotted curve), and $S_{NC}(k)$ (dashed curve) vs $k\sigma_1$ for $x_1=\frac{1}{2}$ and $\Gamma_{\text{eff}}=1.755$.

(jump diffusion), D is expected to vanish at the transition. The recent mode-coupling theories point to a power-law behavior of D in the vicinity of the glass transition.[6,27] Another signature of "structural arrest" is the dramatic increase of the shear viscosity η. In practical MD simulations, the transport coefficients, which are determined by the collective dynamics of the atoms, like η, cannot be obtained with a high degree of accuracy. Moreover, the associated stress tensor autocorrelation function (ACF) builds up a slowly decaying tail as the temperature is lowered, which makes it impossible to obtain even an order of magnitude of η in the supercooled liquid near the transition. For that reason we have concentrated our efforts on the velocity ACF's of the two species in the soft-sphere mixtures, and on the corresponding self-diffusion constants D_α given by[4]

$$D_\alpha=\frac{k_BT}{m_\alpha}\int_0^\infty Z_\alpha(t)dt\ ,$$

$$Z_\alpha(t)=\frac{m_\alpha}{3N_\alpha k_BT}\sum_{i=1}^{N_\alpha}\langle \mathbf{v}_{i\alpha}(t)\cdot\mathbf{v}_{i\alpha}(0)\rangle\ . \tag{24}$$

The short-time expansion of $Z_\alpha(t)$,

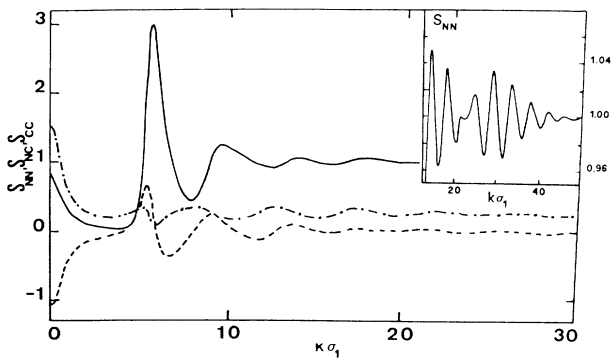

FIG. 7. RY results for the Bhatia-Thornton structure factors at $x_1=\frac{1}{2}$ and $\Gamma_{\text{eff}}=1.943$; symbols have the same meaning as in Fig. 6; the inset shows $S_{NN}(k)$ at large wave numbers on an enlarged scale.

$$Z_\alpha(t)=1-\Omega_{E\alpha}^2\frac{t^2}{2}+O(t^4)\ , \tag{25}$$

involves the characteristic Einstein frequency,

$$\Omega_{E\alpha}^2=\frac{1}{2\pi}\int_{-\infty}^{\infty}\omega^2\hat{Z}_\alpha(\omega)d\omega$$
$$=\frac{1}{3m_\alpha}\sum_\beta\rho_\beta\int g_{\alpha\beta}(r)\nabla^2 v_{\alpha\beta}(r)d\mathbf{r}\ , \tag{26}$$

where $\hat{Z}_\alpha(\omega)$ denotes the power spectrum of the velocity ACF $Z_\alpha(t)$. Physically $\Omega_{E\alpha}$ is the frequency at which an atom of species α vibrates in the potential well of the cage formed by its neighbors fixed at their mean positions $\tau_{E\alpha}=1/\Omega_{E\alpha}$ constitutes the shortest time scale characterizing individual atomic motions. Numerical results for $\Omega_{E\alpha}$ shows that the Einstein frequencies are significantly higher along the glass branch, due to the slightly shorter nearest-neighbor distances compared to the fluid branch (cf. Fig. 4).

Typical velocity autocorrelation functions $Z_1(t)$ and $Z_2(t)$ of an equimolar mixture are shown in Fig. 8 for two states: one near the glass transition, and one deep in the glass phase. As expected, the $Z_\alpha(t)$ exhibit an increasing degree of structure as the temperature is lowered. While the two ACF's exhibit the familiar backscattering effect, followed by a negative plateau in the supercooled fluid state, well-defined oscillations appear

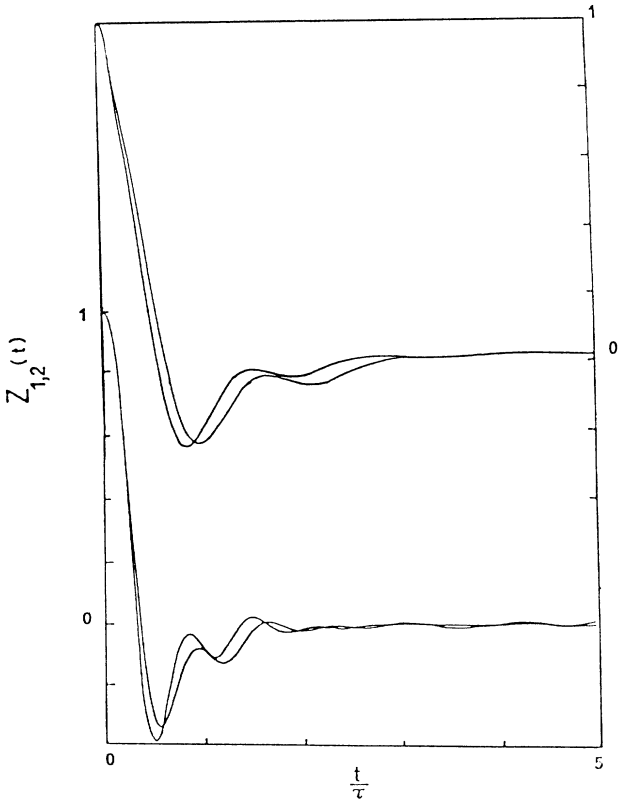

FIG. 8. Velocity autocorrelation functions $Z_1(t)$ (left-most curve) and $Z_2(t)$ vs reduced time t/τ for $x_1=\frac{1}{2}$, $\Gamma_{\text{eff}}=1.51$ (supercooled fluid near the glass transition), and for $\Gamma_{\text{eff}}=1.943$ (low-temperature glass, upper curves).

beyond the glass transition, which are reminiscent of the behavior expected for a harmonic solid. The corresponding spectral functions, for the state close to the glass transition, are shown in Fig. 9; these spectra exhibit well-resolved peaks which are significantly narrower than in the fluid near freezing. Not unexpectedly, the spectra are very sensitive to the mass ratio m_2/m_1. Figure 10 shows the results for the same thermodynamic state as in Fig. 9, but for a mass ratio $m_2/m_1=4$ rather than 2. $\hat{Z}_1(\omega)$ is considerably sharper for the larger mass ratio as a consequence of the cage effect, which is more clear-cut when the large particles are much heavier than the light ones.

We have also computed the interdiffusion current ACF, $J(t)$, which determines the mutual diffusion constant D_{12} according to

$$D_{12}=\frac{k_BT}{m_{12}}\gamma x_1x_2\int_0^\infty J(t)dt \ ,$$

$$J(t)=\frac{m_{12}}{3Nx_1x_2k_BT}\langle \mathbf{j}_{12}(t)\cdot\mathbf{j}_{12}(0)\rangle \ , \tag{27}$$

where $\mathbf{j}_{12}(t)$ is the interdiffusion current

$$\mathbf{j}_{12}(t)=x_2\sum_{i=1}^{N_1}\mathbf{v}_{i1}(t)-x_1\sum_{i=1}^{N_2}\mathbf{v}_{i2}(t) \ , \tag{28}$$

and $\gamma=(\partial^2[G/Nk_BT]/\partial x_1^2)_{P,T,N}$, while $m_{12}^{-1}=x_2m_1^{-1}+x_1m_2^{-1}$. Because it is the ACF of a collective variable, $J(t)$ is affected by considerably larger statistical uncertainties than the velocity ACF. Nonetheless, we find that for all states which were investigated, the calculated $J(t)$ does not differ significantly from the simple superposition

$$J(t)\simeq x_2\frac{m_{12}}{m_1}Z_1(t)+x_1\frac{m_{12}}{m_2}Z_2(t) \ , \tag{29}$$

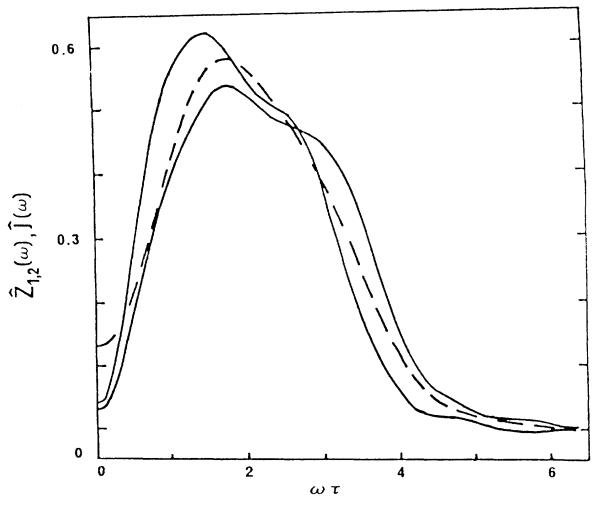

FIG. 9. Spectra $\hat{Z}_1(\omega)$ (right-most solid curve), $\hat{Z}_2(\omega)$ and $\hat{J}(\omega)$ (dashed curve) vs reduced frequency $\omega\tau$ for $x_1=\frac{1}{2}$, $\Gamma_{\text{eff}}=1.51$ and a mass ratio $m_2/m_1=2$ [the corresponding $Z_1(t)$ and $Z_2(t)$ are shown in Fig. 8].

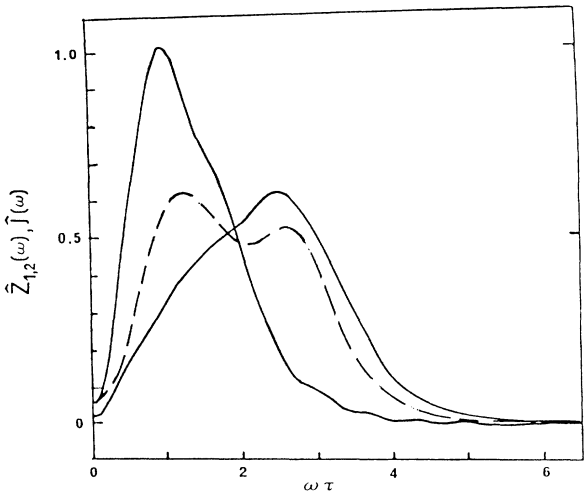

FIG. 10. Same as Fig. 9, but for $m_2/m_1=4$.

which results from complete neglect of the cross correlations between velocities of different particles. Hence, since $\gamma\simeq(x_1x_2)^{-1}$ for nearly ideal mixtures, the interdiffusion constant is approximately given by

$$D_{12}\simeq x_2D_1+x_1D_2 \ , \tag{30}$$

a relation which is reasonably well obeyed in simple liquid mixtures.[28] Spectra $\hat{J}(\omega)$ are shown in Figs. 9 and 10; they agree reasonably well with the simple superposition (29). The results listed in Table III show that, in the supercooled fluid, D_{12} is systematically larger than, but still comparable with, its estimate (30).

Values of the reduced diffusion constants $D_\alpha^*=\sqrt{12}\tau(T^*)^{-5/12}\sigma_1^{-2}D_\alpha$, calculated from Eq. (24), are listed in Table III and plotted in Fig. 11 versus Γ_{eff}: D_1^* and D_2^* are found to drop below the noise level around $\Gamma_{\text{eff}}=1.55$, independently of concentration. However, the estimates of the diffusion constants based on the Kubo relations (24) are unreliable when they become very small, because they result from a near cancellation between positive and negative values of the $Z_\alpha(t)$ (cf. Fig. 8). Under these conditions it is more efficient to estimate directly D_α^* from the Einstein relation

$$\lim_{t\to\infty}\langle\,|\,\mathbf{r}_{i\alpha}(t)-\mathbf{r}_{i\alpha}(0)\,|^2\rangle=\lim_{t\to\infty}\gamma_\alpha(t)=6D_\alpha t \ . \tag{31}$$

The slope of the mean-square displacement $\gamma_\alpha(t)$ of an atom, suitably averaged over all atoms of a given species, allows a more accurate estimate of D_α than an integration of $Z_\alpha(t)$, when the resulting integral is small, due to the unavoidable inclusion of statistical noise at long times. The time dependence of the mean-square displacements of the two species is shown in Fig. 12 for three thermodynamic states in the vicinity of the glass transition. At the highest temperature, $\gamma_\alpha(t)$ reaches its asymptotic (linear) regime rapidly, typically after 10–20 Einstein periods $\tau_{E\alpha}$. This behavior is observed throughout the stable and supercooled fluid range, up to $\Gamma_{\text{eff}}\simeq 1.4$. At lower temperatures, as the glass transition

TABLE III. Self- and mutual diffusion constants, calculated from the Kubo relations (24) and (27) (K) or from the Einstein limit (31) (E).

MD	x_1	Γ_{eff}	$10^2 D_1^*$	$10^2 D_2^*$	$10^2 D_{12}^*$	$10^2(x_2 D_1^* + x_1 D_2^*)$
			$m_2/m_1=2$			
E	0.5	0.947	8.6(E)	5.7(E)		
E	1.0	1.131	2.95(E)			
E	0.5	1.143	3.6(K)	2.0(K)	4.0	2.8
E	0.5	1.154	3.0(K)	1.9(E)		
E	0.25	1.156	3.8(K)	2.1(K)	5.0	3.4
E	0.75	1.192	2.3(K)	1.3(K)	2.6	1.6
E	0.5	1.221	2.2(K)	1.15(K)	2.2	1.7
E	0.5	1.280	1.5(K)	0.72(K)	1.3	1.1
E	0.5	1.352	0.82(E)	0.38(E)		
E	0.9	1.376	0.19(K)	0.10(K)	0.18	0.11
E	0.5	1.418	0.42(K)	0.23(K)	0.78	0.33
T	0.5	1.425	0.39(K) 0.42(E)	0.19(K) 0.18(E)		
E	0.5	1.494	0.13(K)	0.06(K)	0.12	0.095
E	0.5	1.508	0.11(K)	0.03(K)		
E	0.5	1.523	0.07(K) 0.10(E)	0.02(K) 0.025(E)		
T	0.5	1.523	0.13(K) 0.10(E)	0.06(K) 0.04(E)		
E	0.25	1.571	0.085(K)	0.03(K)		
E	0.5	1.586	0.04(K) 0.03(E)	0.015(K) 0.013(E)		
T	0.5	1.584	0.045(K) 0.03(E)	0.02(K) 0.01(E)		
T	0.5	1.670	0.005(E)	0.001(E)		
			$m_2/m_1=4$			
E	0.5	1.242	1.64(K)	0.98(K)	1.5	1.3
E	0.5	1.451	0.28(K)	0.22(K)	0.35	0.25
E	0.5	1.511	0.10(K)	0.05(K)	0.16	0.075

is approached, $\gamma_\alpha(t)$ exhibits significant curvature out to increasingly long times, and reaches the linear regime only after more than 100 Einstein periods. This renders an accurate determination of the slope $6D_\alpha$ very difficult. In particular, if $\gamma_\alpha(t)$ is not extended to sufficiently long times, D_α is easily overestimated, due to the negative curvature of $\gamma_\alpha(t)$ at intermediate times. A similar "subdiffusive" behavior is clearly apparent in our simulations of the supercooled one-component soft-sphere fluid,[11] and in a recent MD study of supercooled fluids of atoms interacting through a repulsive Yukawa potential.[29]

Another manifestation of the non-Gaussian nature of self-diffusion near the glass transition can be found in the time dependence of the ratios

$$R_\alpha(t)=\frac{3\langle |\mathbf{r}_{i\alpha}(t)-\mathbf{r}_{i\alpha}(0)|^4\rangle}{5[\langle |\mathbf{r}_{i\alpha}(t)-\mathbf{r}_{i\alpha}(0)|^2\rangle]^2} . \tag{32}$$

For a purely Gaussian process, $R_\alpha(t)=1$ for all times. For simple liquids near freezing, $R_\alpha(t)$ deviates from 1 at most by 10%.[30] However, our MD data show that $R_\alpha(t)$ becomes increasingly non-Gaussian as the temperature is lowered towards the glass transition. As shown in Fig. 13, the amplitude of the maximum deviation of $R_\alpha(t)$ from 1 increases dramatically near the transition, and this maximum is reached more and more slowly. This highly non-Gaussian behavior is reminiscent of jump diffusion process occurring in superionic conductors[31] and underlines the importance of activated processes near the glass transitions.

Figure 11 shows that the self-diffusion constants D_1^* and D_2^* obey reasonably well an Arrhenius law

$$D_\alpha^* = A_\alpha \exp(-a_\alpha/T) = A_\alpha \exp(-b_\alpha \Gamma_{\text{eff}}^4) , \tag{33}$$

where for $x_1=0.5$, $A_1=0.18$, $b_1=1.0$, and $A_2=0.15$, $b_2=1.1$. It is interesting to note that the data for other concentrations and for equimolar mixtures with a mass ratio $m_2/m_1=4$, fall roughly on the same Arrhenius lines. The slope of the lines corresponding to the two species is slightly different, so that the ratio D_1/D_2 increases as the temperature is lowered, from about 1.7 near freezing to nearly 3 in the vicinity of the glass transition. In light of recent predictions of mode-coupling theory, we have also examined the validity of a scaling law of the type

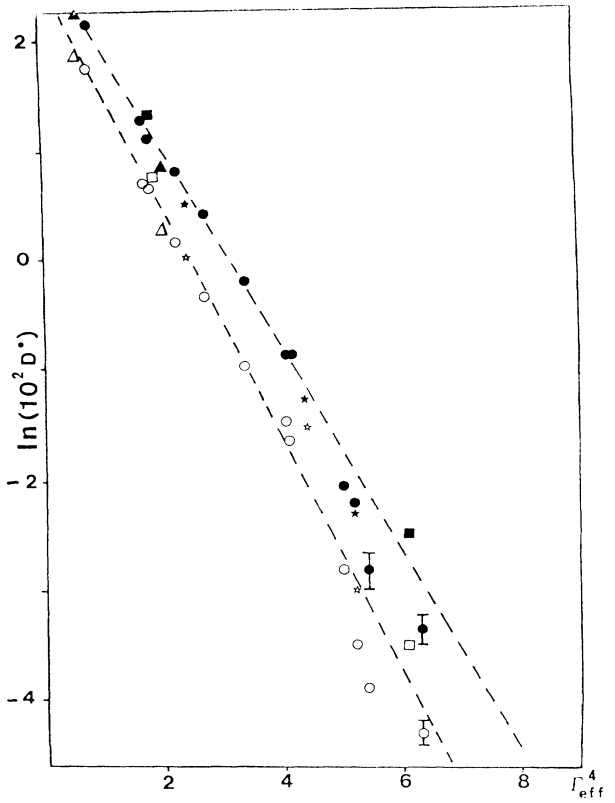

FIG. 11. Arrhenius plot of the reduced diffusion constants D_1^* (solid symbols) and D_2^* (open symbols). Triangles, $x_1=0.75$; circles, $x_1=0.5$; squares, $x_1=0.25$. The stars are for $x_1=0.5$ and the larger mass ratio $m_2/m_1=4$; note the deviations from Arrhenius behavior (materialized by the dashed straight lines) at the lower temperatures (large Γ_{eff}); the vertical bars indicate rough estimates of statistical uncertainties, based on the difference between the Kubo and Einstein routes to D_α^*.

$$D_\alpha^* = B_\alpha(\Gamma_g - \Gamma)^{\nu_\alpha} . \tag{34}$$

The best fit for equimolar mixtures, shown in Fig. 14, is obtained for $\Gamma_g=0.87$ ($\Gamma_{eff}=1.566$) and $\nu_1=\nu_2\simeq 2$. The exponent ν is practically the same for the two species, and agrees reasonably well with the predictions of mode-coupling theory for a one-component Lennard-Jones system ($\nu\simeq 1.6-1.8$).[6,27] The overall quality of the fit (34) is at least as good as the Arrhenius fit (33). The scaling law (34) is inapplicable in the immediate vicinity of the glass transition, where activated processes lead to a small residual diffusion, even beyond the transition, as is clear from Table III.

VI. DISCUSSION

By considering binary mixtures, we have been able to perform extensive molecular-dynamics computer "experiments" on supercooled and amorphous states of a soft-sphere model which showed no tendency towards nucleation. Our results show some of the characteristic features that are familiar from previous simulations of one-component "computer glasses," but we believe that

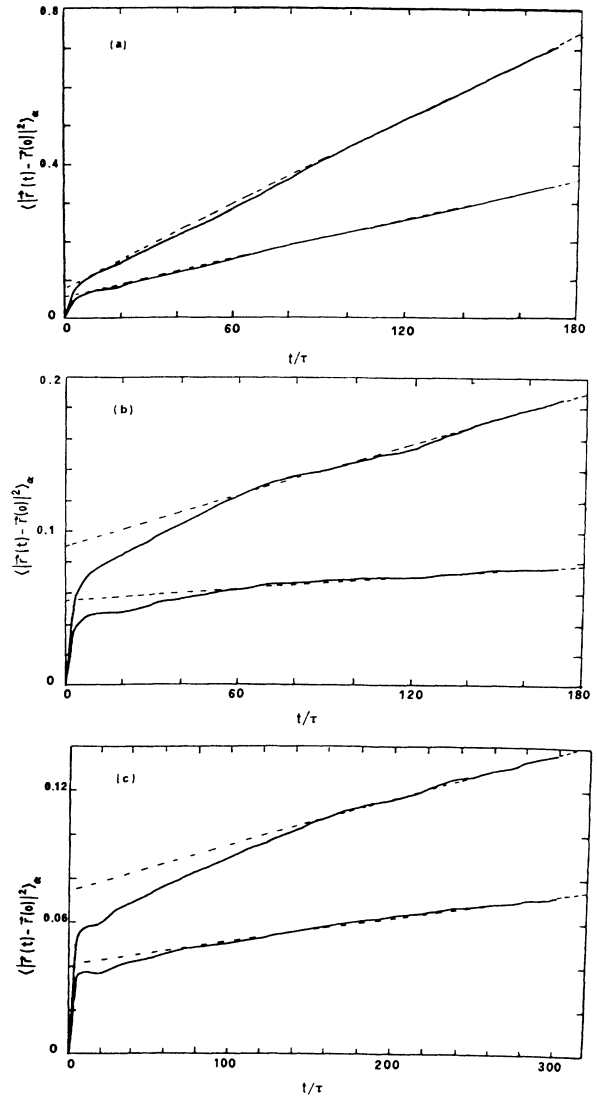

FIG. 12. (a) Mean-square displacements (in units of σ_1) of the light (upper curve) and heavy particles vs reduced time for $x_1=\frac{1}{2}$, $\Gamma_{eff}=1.425$; the dashed straight lines are the estimated asymptotes. (b) Same as (a), but for $\Gamma_{eff}=1.523$. (c) Same as (a) but for $\Gamma_{eff}=1.584$.

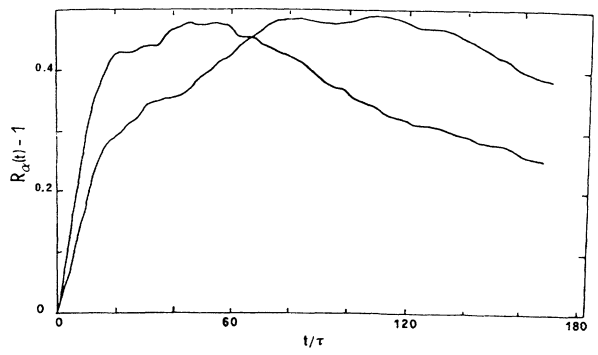

FIG. 13. "Non-Gaussian" ratio $R_\alpha(t)$ for the lighter (leftmost curve) and heavier particles vs reduced time for $x_1=\frac{1}{2}$, $\Gamma_{eff}=1.425$.

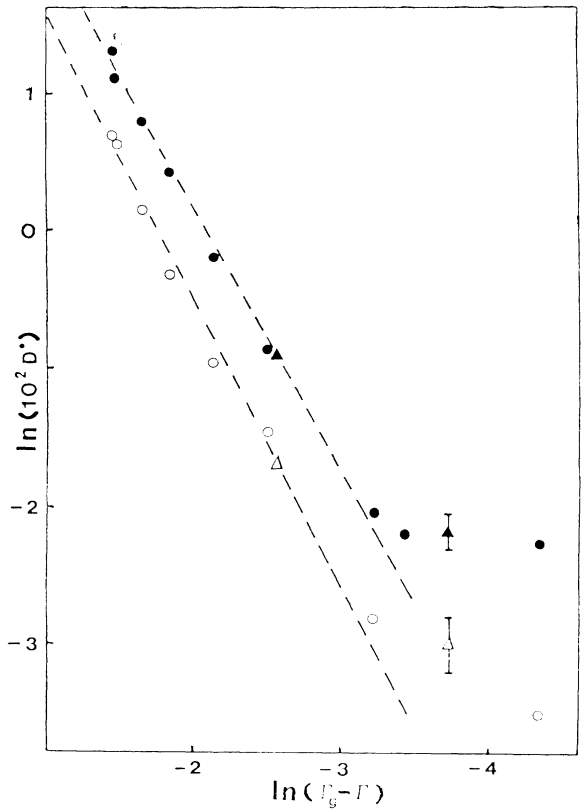

FIG. 14. Power-law plot of the reduced self-diffusion constant D_1^* (solid symbols) and D_2^* (open symbols). The circles are from constant-energy MD simulations, while the triangles are from constant-temperature simulations. The slopes of the dashed lines are close to 2. Note the strong deviations from the power-law behavior (34) close to the glass transition due to activated processes.

two of our main findings are novel, to the best of our knowledge. The first result is clear evidence for a bifuraction of the equation of state into "giass" and "fluid" branches below the transition temperature T_g. Although such a bifurcation is frequently postulated in the literature on the glass transition, our MD computations and the solutions of the thermodynamically self-consistent RY integral equation yield convincing theoretical evidence for the simultaneous existence of quenched amorphous and fully relaxed fluid states. The fluid branch is found to lead to phase separation at very low temperatures. This opens the possibility of studying the phase separation observed experimentally in many multicomponent glass-forming systems.[32]

The second important result of our MD simulations is the emergence of an intermediate time scale in the mean-square displacement of the atoms near the glass transition. Between the initial rapid atomic motion in the cage of nearest neighbors and the linear diffusion regime at sufficiently long times, the mean-square displacement is characterized by a highly non-Gaussian, subdiffusive time dependence which extends over 10^2 Einstein periods or more. We believe that this regime is intimately related to the slowing down of structural relaxation. The small, residual diffusion observed below the glass transition temperature is due to activated processes (jump diffusion) which exist even if the structure is frozen. This "rounding off" of the transition is in qualitative agreement with a recent theoretical analysis of Das and Mazenko.[33] Discarding this residual diffusion, the diffusion constants of the two species obey over the whole supercooled fluid domain a simple scaling law of the form (34) with an exponent ν nearly equal to 2. In a subsequent paper we shall present a direct investigation of structural slowing down based on MD results for the density autocorrelation function.

ACKNOWLEDGMENTS

The authors are grateful to the Conseil Scientifique du Centre de Calcul Vectoriel pour la Recherche (Palaiseau, France) for a generous allocation of computer time and to Direction des Recherches et Etudes Techniques (DRET) for financial support under Contract No. 84/132. Some of the computations were carried out on the Digital Equipment Corporation VAX 11/750 minicomputer of Ecole Normale Supérieure with the support of the GRECO Expérimentation Numérique. Y.H. thanks the Japanese Society for the Promotion of Science (JSPS) and a grant-in-aid for science research by the Ministry of Education, Science and Culture (Japan) for their financial support. G. P. thanks the Consiglio Nazionale delle Ricerche (Italy) for support. Laboratoire de Physique Théorique des Liquides is Unité associée au Centre National de la Recherche Scientifique (France).

*Permanent address: International School for Advanced Studies, I-34014 Trieste, Italy.

[1]For a review, see C. A. Angell, J. H. R. Clarke, and L. V. Woodcock, Adv. Chem. Phys. **48**, 397 (1981).
[2]J. R. Fox and H. C. Andersen, J. Chem. Phys. **88**, 4019 (1984).
[3]S. Nosé and F. Yonezawa, Solid State Commun. **56**, 1005 (1985).
[4]J. P. Hansen and I. R. McDonald, *Theory of Simple Liquids*, 2nd ed. (Academic, London, 1986).
[5]E. Leutheusser, Phys. Rev. A **29**, 2765 (1984).
[6]U. Bengtzelius, W. Götze, and A. Sjölanger, J. Phys. C **17**, 5915 (1984).
[7]W. Götze, Z. Phys. B **60**, 195 (1985).
[8]T. R. Kirkpatrick, Phys. Rev. A **31**, 939 (1985).
[9]W. Götze and L. Sjögren, J. Phys. C **20**, 879 (1987).
[10]J. J. Ullo and S. Yip, Phys. Rev. Lett. **54**, 1509 (1985).
[11]Y. Hiwatari, B. Bernu, and J. P. Hansen (to be published).
[12]B. Bernu, Y. Hiwatari and J. P. Hansen, J. Phys. C **18**, L371 (1985); J. Phys. (Paris) Colloq. Supplement No. 12, **46**, C8-323 (1985).

[13]J. P. Hansen, Phys. Rev. A **2**, 221 (1970).
[14]W. G. Hoover, M. Ross, K. W. Johnson, D. Henderson, J. A. Barker, and B. C. Brown, J. Chem. Phys. **52**, 4931 (1970).
[15]Y. Hiwatari, Prog. Theor. Phys. **53**, 915 (1975).
[16]Y. Hiwatari, J. Phys. Soc. Jpn. **47**, 733 (1979).
[17]J. N. Cape and L. V. Woodcock, J. Chem. Phys. **72**, 976 (1980).
[18]F. J. Rogers and D. A. Young, Phys. Rev. A **30**, 999 (1984).
[19]B. Bernu, Physica **122A**, 129 (1983).
[20]W. G. Hoover, A. J. C. Ladd, and B. Moran, Phys. Rev. Lett. **48**, 1818 (1982); W. G. Hoover, Physica **118A**, 111 (1983).
[21]S. Nosé, J. Chem. Phys. **81**, 511 (1984).
[22]J. P. Hansen and G. Zerah, Phys. Lett. **108A**, 277 (1985).
[23]Y. Hiwatari and H. Matsuda, Prog. Theor. Phys. **47**, 741 (1972).
[24]M. Kac, G. E. Uhlenbeck, and P. C. Hemmer, J. Math. Phys. **4**, 216 (1963).
[25]J. L. Lebowitz and O. Penrose, J. Math. Phys. **7**, 98 (1966).
[26]A. B. Bhatia and D. E. Thornton, Phys. Rev. B **2**, 3004 (1970).
[27]U. Bengtzelius, Phys. Rev. A **33**, 3433 (1986).
[28]G. Jacucci and I. R. McDonald, Physica **80A**, 607 (1975).
[29]K. Kremer, G. S. Grest, and M. O. Robbins, J. Phys. A **20**, L181 (1987).
[30]A. Rahman, Phys. Rev. **136**, A405 (1964).
[31]M. J. Gillan and M. Dixon, J. Phys. C **13**, 1901 (1980).
[32]W. Vogel, J. Non-Cryst. Solids **25**, 172 (1977).
[33]S. Das and G. Mazenko, Phys. Rev. A **34**, 2256 (1986).